Plant Methods

METHODOLOGY

Open Access

An optimized pipeline for live imaging whole *Arabidopsis* leaves at cellular resolution

Kate Harline[1,2] and Adrienne H. K. Roeder[1,2*]

Abstract

Background Live imaging is the gold standard for determining how cells give rise to organs. However, tracking many cells across whole organs over large developmental time windows is extremely challenging. In this work, we provide a comparably simple method for confocal live imaging entire *Arabidopsis thaliana* first leaves across early development. Our imaging method works for both wild-type leaves and the complex curved leaves of the *jaw-1D* mutant.

Results We find that dissecting the cotyledons, affixing a coverslip above the samples and mounting samples with perfluorodecalin yields optimal imaging series for robust cellular and organ level analysis. We provide details of our complementary image processing steps in MorphoGraphX software for segmenting, tracking lineages, and measuring a suite of cellular properties. We also provide MorphoGraphX image processing scripts we developed to automate analysis of segmented images and data presentation.

Conclusions Our imaging techniques and processing steps combine into a robust imaging pipeline. With this pipeline we are able to examine important nuances in the cellular growth and differentiation of *jaw-D* versus WT leaves that have not been demonstrated before. Our pipeline is approachable and easy to use for leaf development live imaging.

Keywords Live imaging, Computational image analysis, Arabidopsis, Leaf, Morphogenesis, Growth, Vegetative development, MorphoGraphX

Background

The beautiful variety of life-forms on Earth arise from differential growth in three dimensions. Leaves offer a system to study the cellular and genetic basis of this process because they exhibit a wide range of different forms and exhibit dynamic heterogeneous growth [1–6]. Advances in imaging techniques now allow us to track this development from the first few cells that initiate an organ [7–10]. Further, cellular resolution of the same plants allows for the parameterization and fitting of models that can give greater insights into developmental processes than time-point sampling of different plants [11–13].

Yet, complex forms, like the rippling and waving leaves of the mutant *jaw-D* can stymie research by creating intractable systems for imaging [14]. Due to its curved nature, the *jaw-D* leaf surface is particularly difficult to image in its entirety while keeping the plant alive because the leaf surface occludes itself. Similar issues arise in many other Arabidopsis mutants featuring curvature mutations, for example: *peapod, incurvata* and *curly leaf* [15–17]. Optical sectioning in plant tissues is often limited to the first one to two layers due to the density of plant tissue, airspaces in between cells and autofluorescence induced by chlorophyll, so imaging through curved parts is not currently feasible [18]. Further, even if images can be acquired, increased imaging in the z-direction

*Correspondence:
Adrienne H. K. Roeder
ahr75@cornell.edu
[1] Weill Institute for Cell and Molecular Biology, Cornell University, Ithaca, NY 14853, USA
[2] Section of Plant Biology, School of Integrative Plant Sciences, Cornell University, Ithaca, NY 14853, USA

comes at a time cost which can threaten sample viability. We therefore aimed to create an imaging pipeline that would minimize information lost due to tissue deformation in the z-direction while also minimizing time per sample.

In this pipeline, we have synthesized strategies from leading live and fixed imaging protocols to obtain a robust system for measuring the development of morphologically complex whole plant leaves [7, 10, 19–21]. Our method also makes imaging morphologically simple (relatively flat) samples easier, and permits fewer sample manipulations between imaging time points. We believe these strategies can be applied to a variety of plant tissues to improve time lapse image capture.

Results and discussion

Method improvements

In order to study the development of leaf primordia, we image leaves as they emerge from the shoot apical meristem. We plate seeds on phytoagar-based growth media, then allow them to germinate in the growth chamber for 2–3 days (hereafter, DAS). We then dissect the cotyledons off of the plants and allow them to recover for one day before beginning imaging (Fig. 1). Before imaging we also affix a coverslip above the samples. This helps keep the samples in an ideal position for imaging. With coverslips affixed we found that perfluorodecalin is an ideal mounting media to keep samples alive and maintain image quality.

We image the same plants this way for at least six days. Our samples contain a small plasma membrane-localized protein tagged with a fluorescent protein, so we are able to get high resolution images of every cell border in these images. This allows us to track the creation of recognizable leaf tissue containing thousands of cells from an initial unrecognizable nub of tens of cells [22]. Our samples grow from hundreds of micrometers in area to millimeters in area, so they quickly exceed the single 20 × imaging window at which the plasma membrane marker is resolvable (~ 5 DAS). We thus manually acquire tiles of smaller parts of our samples and then reassemble these individual tiles in MorphoGraphX software (see Methods for tiling details). We then use MorphoGraphX to convert this raw fluorescent signal into an object the computer can recognize. This involves masking the raw confocal signal, then fitting a curved surface to this mask, re-projecting the raw signal onto this surface and segmenting the signal into computer-recognized cell outlines (see Additional file 6: annotated_task_list.docx). With this segmented mesh, we can directly measure and quantify the growth, divisions and changes in morphology of the same cell lineages throughout the imaging period. We developed scripts to speed up the processing and downstream quantification steps. The combination of these technical improvements, computational resources and our detailed supplemental information makes our pipeline ideal for researchers that are interested in tissues that curve and fold and especially newcomers to live imaging.

Tissues grown beneath coverslips are more amenable to imaging

Plants grown in agar have a natural tendency to shift over time because the roots grow gravitropically and subsequent leaves emerge from the meristem. These developmental events shift the sample in the plate. As early leaf development proceeds, the three dimensionality of leaves becomes more apparent and imaging their entirety becomes more difficult (Fig. 2). Early leaf development includes a bend that develops between the petiole and leaf blade in almost all leaves and a variety of curvature and margin patterning differences amongst mutant lines [14–16, 23](Figs. 1F, 2A, C). This can be an issue because it can lead cells from a previous time point to become obscured. These cells cannot be tracked between time points, their growth and cell division rates cannot be measured, and thus must be removed from the dataset. In order to maximize the surface of the tissue that could be imaged and tracked, while minimizing time lost to traversing z-steps, we experimented with growing plants beneath coverslips (Figs. 1C–E, 2B, D). Imaging and growing plants beneath coverslips offered many benefits to the pipeline. Leaves grown beneath coverslips shift much less in the plate overall and especially less in the z-dimension (Fig. 2). This minimized plant movement in between imaging sessions and the risk of sample damage upon re-positioning.

It also lowered the time each sample took to image by decreasing the z-step range. Further, cells were no longer lost due to tissue flipping.

Additionally, contamination of agar plates is a concern while conducting live imaging experiments. Plates will be exposed to open air for upwards of 3 h. Some researchers use fungal inhibitors to prevent contamination [7]. These treatments can reduce growth (Personal communication, Dr. Lilan Hong, Zhejiang University). Other researchers opt to replace media regularly via complex microfluidic devices, by manual transplantation to fresh plates each day or with nutrient-minimal media [8–10]. We have found that growing plants beneath coverslips radically reduces the contamination that occurs over the week or more that plants are growing. Only once in all of the weeklong experiments conducted was mold found beneath the coverslip. This is a benefit as it again reduces the threat of damaging the samples from replating or losing cells by imperfect re-positioning.

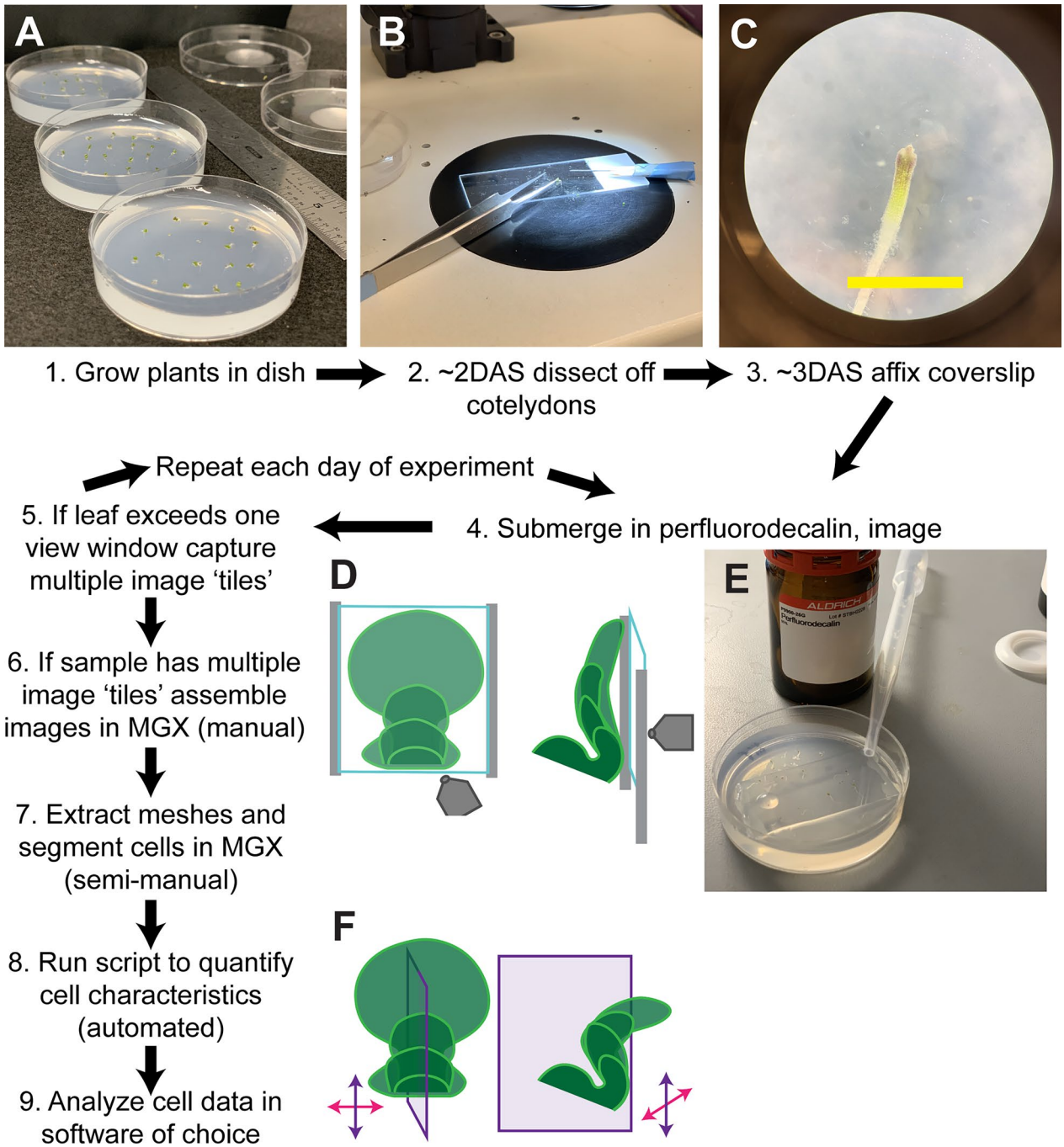

Fig. 1 Sample preparation. **A** Germinated Arabidopsis seedlings on agar plates immediately before dissection. **B** General dissection setup under stereoscope for a right-handed researcher. Seedlings can be dissected within the plate or moved to a glass slide to dissect off cotyledons. **C** Stereoscope image under 50 × magnification of sample post-dissection, 3 DAS (Days after sowing). Yellow scale bar = 2 mm. **D** Schematic of positions of coverslip (blue square), grease strips for cover-slip suspension (gray lines) and microscope objective (gray shape, not to scale). The leaf blade flattens along the affixed coverslip. **E** One plate with all samples dissected, below suspended coverslip and immersed in perfluorodecalin (PFD). **F** Schematic of leaf growth without a coverslip. The abaxial surface naturally curves perpendicularly out from the plate. Directions relative to the proximal–distal and medial–lateral axes indicated with purple or magenta arrows, respectively. Purple plane indicates the cross-section displayed on the right

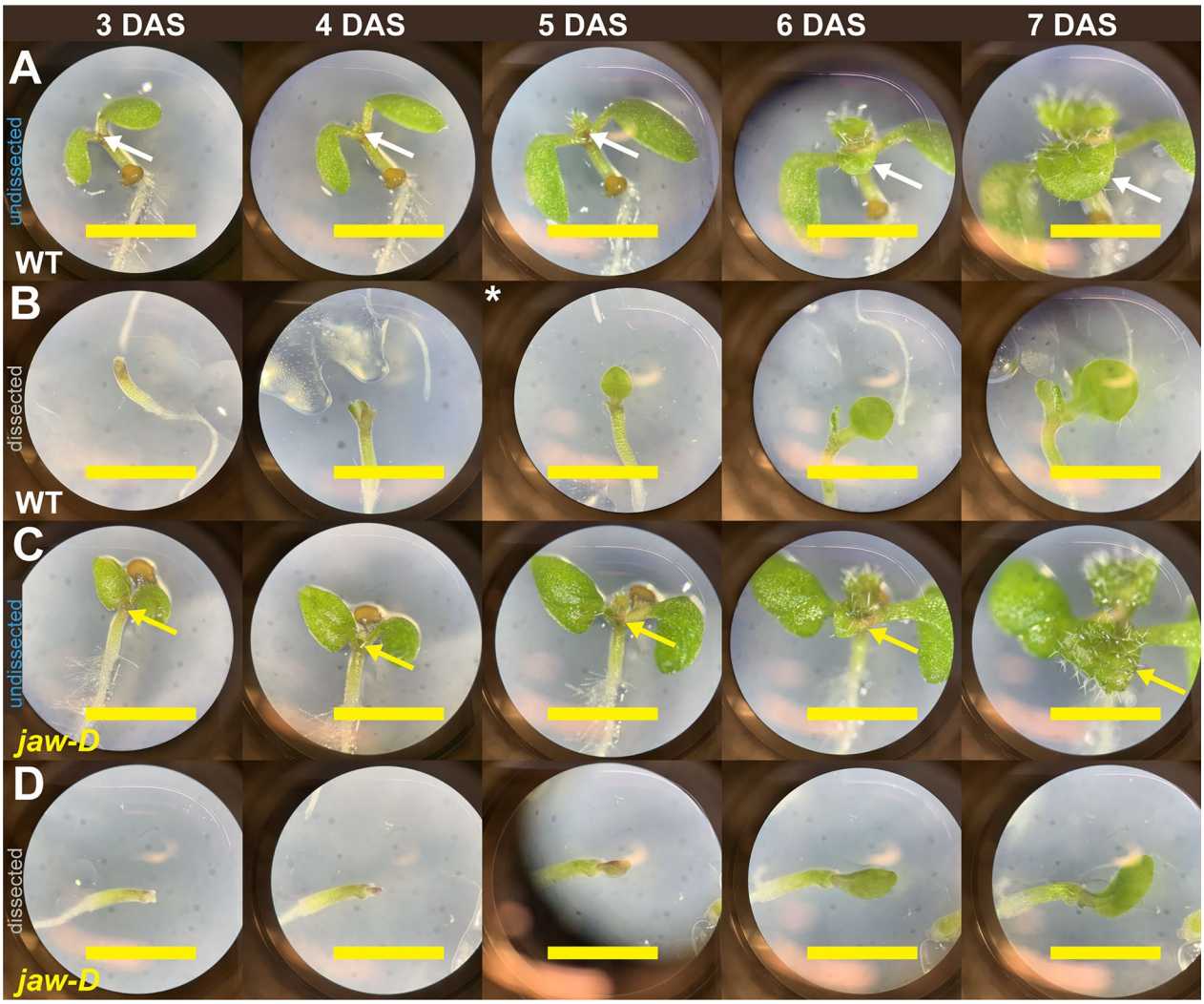

Fig. 2 Sample growth and curving during the live imaging experiment. Stereoscope images at 50 × magnification of leaf samples with no coverslip and also no cotyledon dissection **A**, **C** or samples with dissection and affixed coverslip **B**, **D** for the same* WT (**A**–**B**, white) and *jaw-D* (**C**–**D**, yellow) samples over the course of a live imaging experiment. Dissected samples affixed with a cover slip maintain positions with more exposed leaf tissue for imaging over time. Both WT and *jaw-D* leaves begin to grow out from the plate without coverslip dissection exposing the adaxial side. This is especially true in *jaw-D* where the tissue becomes curled around itself at 7 DAS. *5 DAS image was missing for this sample so an image from a different WT leaf sample is provided. Arrows indicate leaf that was imaged. Yellow scale bars = 2 mm

Dissecting cotyledons exposes more cells without impacting growth

Within 48 h of being placed in the growth chamber, the cotyledons of Arabidopsis will emerge from the seed and begin to open. By this time, the first true leaves will have been initiated (Fig. 2). However, due to the presence of the cotyledons, the earliest development of the first two true leaves is obscured. Previous efforts have dealt with this problem in a few ways. Regions obscured by the cotyledons have been dropped from the potential dataset [8]. Images have been taken later in the development of the leaf once more of the blade has emerged [5]. Or, dissections have been performed to remove cotyledons or older leaves [7, 10]. In accord with this last strategy, we experimented with dissecting off one and two cotyledons (Figs. 1B, C, 2B, D, 3). We grew WT plants with and without the cotyledons dissected in the same plates to control for condition variation (Figs. 3, 4). We tested to what extent dissections improved tissue exposure for imaging and checked that growth and cell divisions were not impaired in dissected samples. Upon dissection,

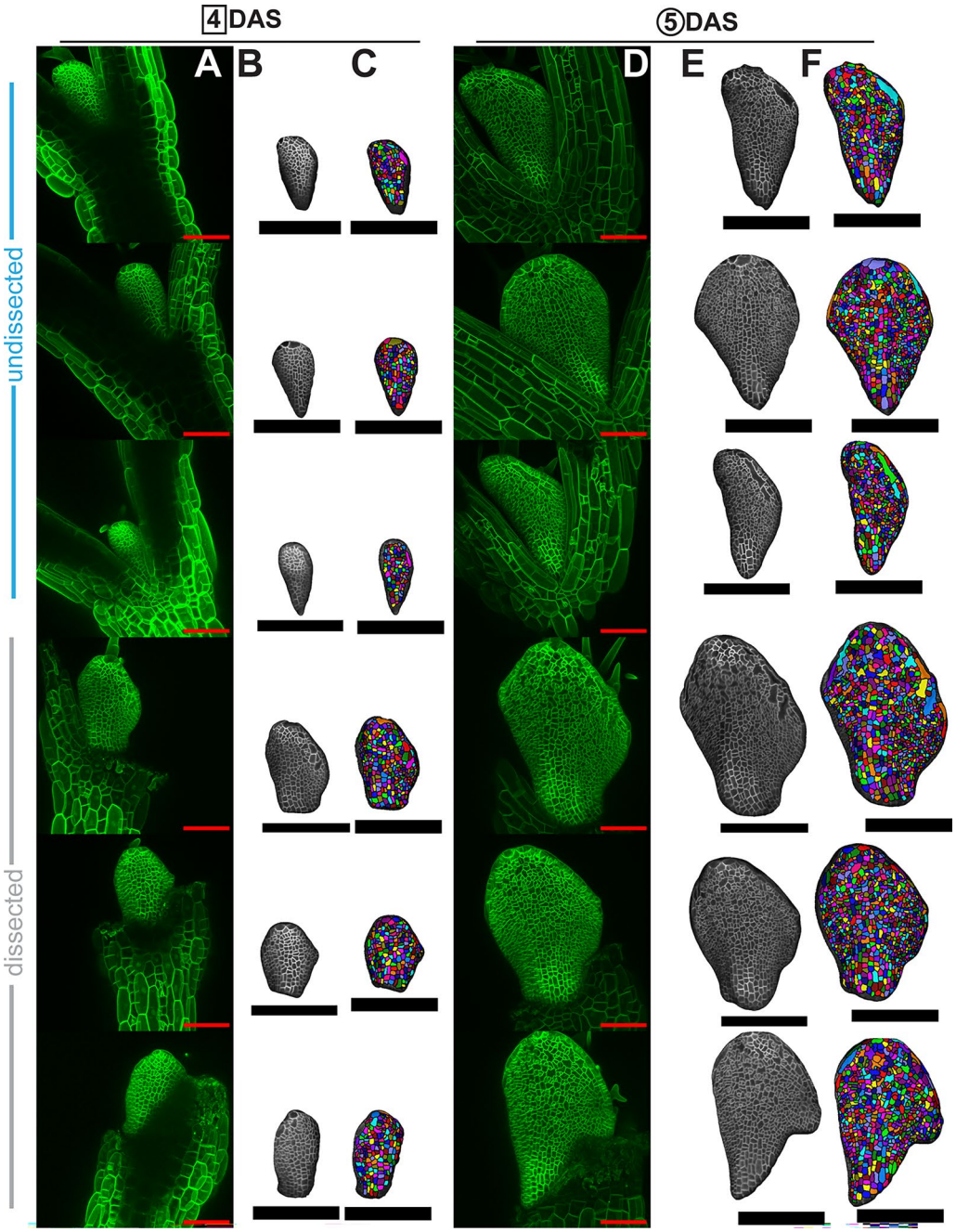

Fig. 3 Dissecting cotyledons increases imaging accessibility. Comparison of exposed and segmentable cells in undissected (top three rows) versus dissected (bottom three rows) samples for the sample replicates from 4 DAS (**A**–**C**) to 5 DAS (**D**–**F**). More cells and more of the basal petiole and margin regions are accessible in the dissected samples. **A**, **D** Raw confocal images as maximum intensity projections. **B**, **E** Snapshots of the same images rendered as 2.5D meshes in MorphoGraphX 2.0. **C**, **F** Snapshots of the same meshes with segmentable cells indicated with unique colored labels and outlined in black. Red scale bars = 100 µm. Black scale bars = 200 µm

more cells along the early primordial margin and base are revealed and amenable to segmentation (Figs. 3, 4A–D). Importantly, there is no significant difference in the areal growth or cell divisions between dissected and undissected samples (Fig. 4E–H) .

Perfluorodecalin maintains samples over many days

In our early experiments we used water based solutions to immerse the samples. The leaf growth stalled, possibly because these solutions often absorb into the media and can form a vacuum with the coverslip (Fig. 5, Additional

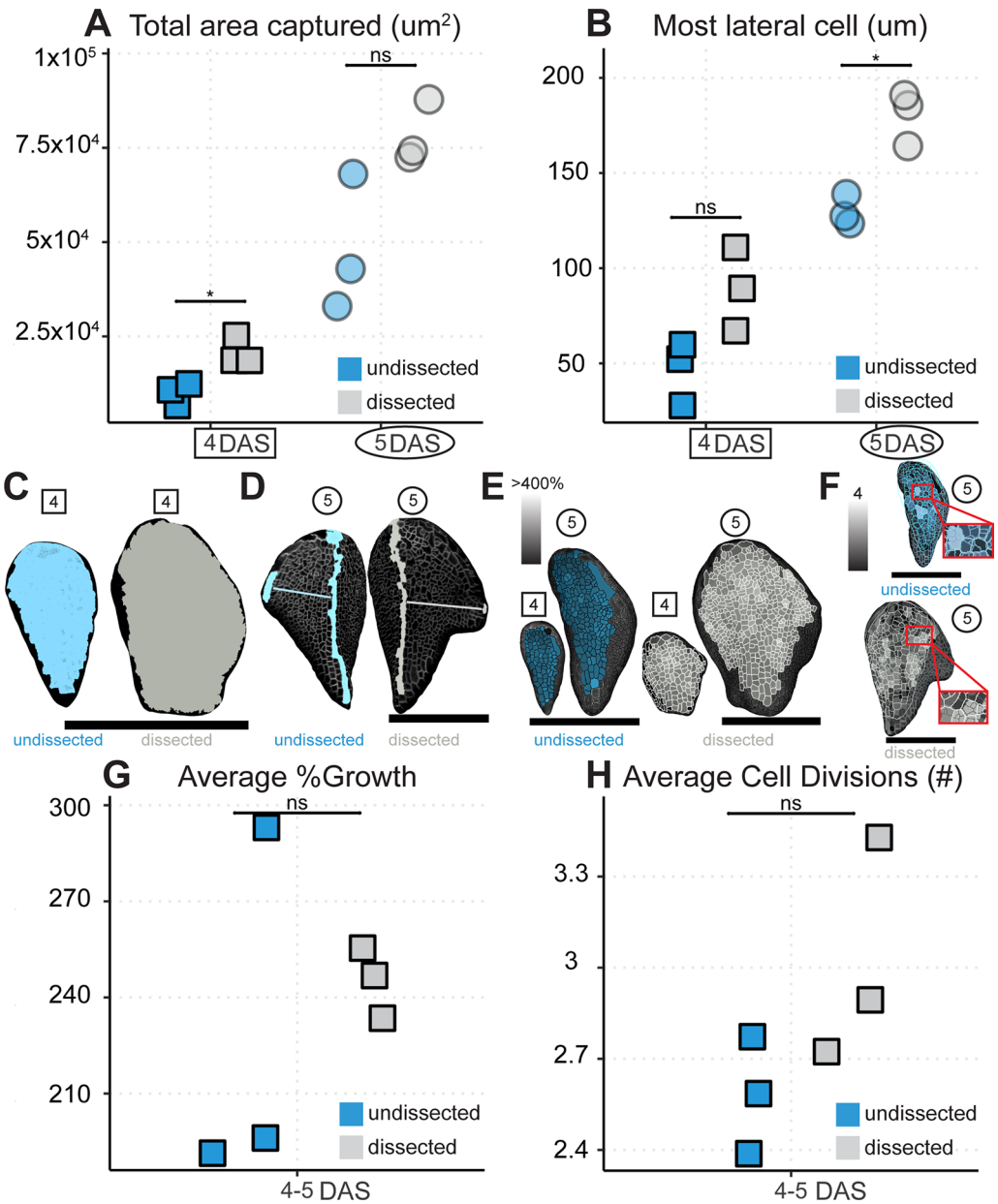

Fig. 4 Dissecting cotyledons increases imaging accessibility without altering growth and cell divisions. Quantification of the segmentable area **A** and most lateral cell captured **B** from the three replicates in Fig. 3 at 4 DAS (squares) and 5 DAS (circles). Dissected samples (gray) trend towards or have significantly more segmentable area and furthest lateral cells exposed for imaging than undissected samples (blue). (Student's t-tests, * = $p < 0.05$). **C** The largest total area captured for each condition at 4 DAS represented on its respective mesh. **D** The furthest lateral cell for each condition, undissected (blue) or dissected (gray), at 5 DAS shown on its respective mesh. Medial cells are also selected with a line drawn for distance reference. Note how the dissected sample's most lateral cell is lower in the tissue so more marginal cells can be captured through dissection. **E** Cell areal growth from 4–5 DAS represented on the 4 and 5 DAS meshes for the sample with the median value of average growth for each condition. **F** Cell divisions from 4–5 DAS shown on the 5 DAS mesh for the sample with the median value of average divisions for each condition. The corresponding 4 DAS mesh is scaled and overlaid to show the parent cell outline for daughter cell clones. Insets are zoomed views. **E**–**F** Light- er shading indicates more growth (percent area increase) or divisions (#) as indicated. Average growth **G** or number of cell divisions **H** from 4–5 DAS for each replicate. Average growth and divisions are not statistically different between treatments, so dissection does not interfere with regular development (Student's t-test $p > 0.05$). Black scale bars = 200 µm. See Table 1 for replicate cell counts.

Table 1 Cells measured in dissection v. no dissection (Fig. 4)

Condition	Time point	Number of cells
undissected	4 DAS (also 4–5 DAS)	369
undissected	5 DAS	1493
dissected	4 DAS (also 4–5 DAS)	618
dissected	5 DAS	2091

file 3: Video S3). This prompted us to search for other immersion solutions with high refractive index to maintain good imaging resolution while not leading to tissue stalling. We attempted imaging with glycerol, iodixanol and perfluorodecalin (PFD). We found that PFD had the best results in maintaining image quality. PFD is known to permit the dissolution of gasses like oxygen and carbon dioxide, which likely contributes to its prevention of tissue stalling [24]. Notably, PFD is also slippery and absorbs into the media much less, so it is easier to remove in between imaging sessions.

Development of MorphoGraphX scripts increases image processing and analysis efficiency

Image processing, cell segmentation and lineage tracking can be a laborious and time intensive process (see Image Processing in the Section "Materials and Methods" and Additional file 6: annotated_task_list.docx). We therefore aimed to make the final image data analysis as efficient

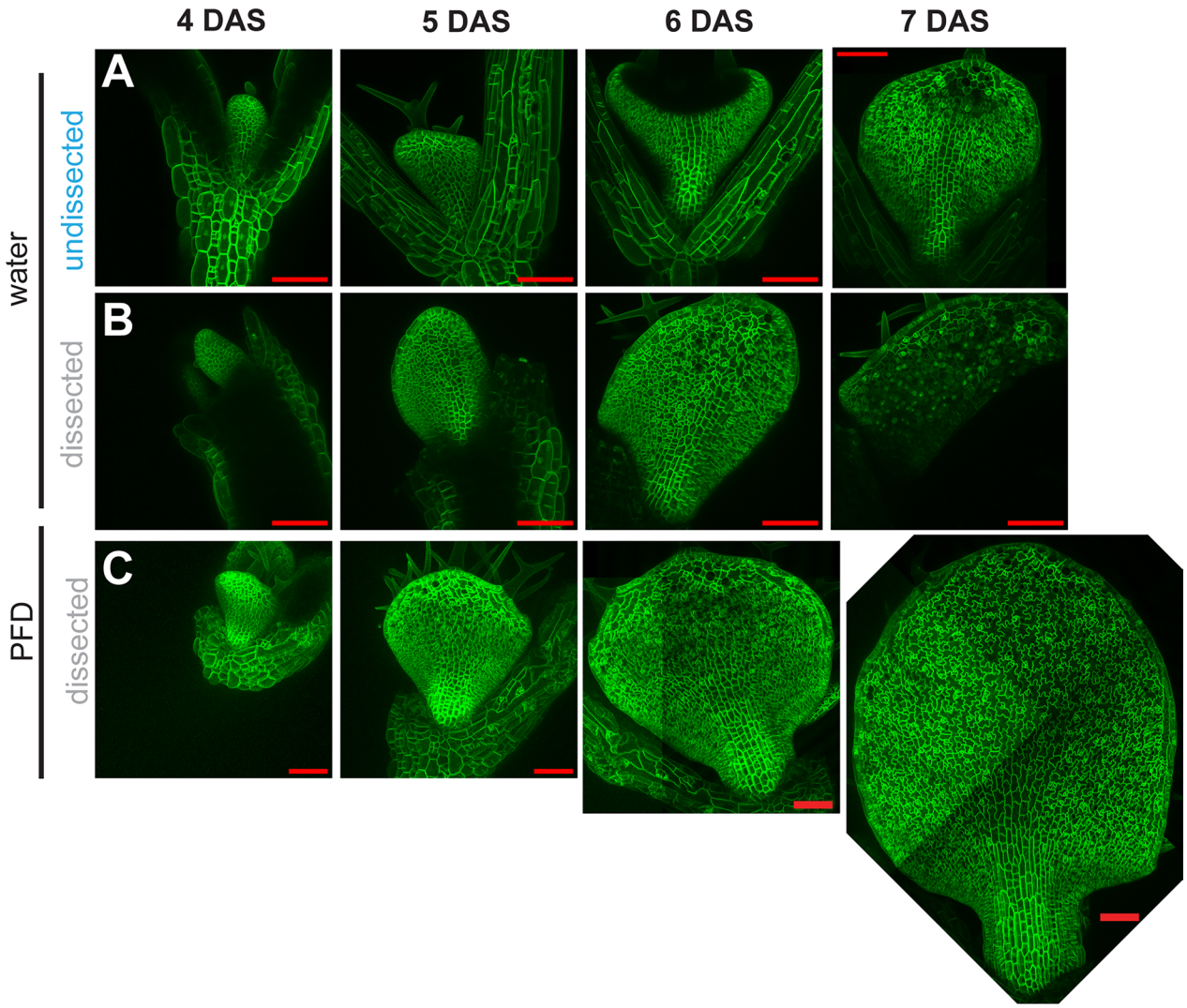

Fig.5 PFD allows long term imaging of samples under coverslips Confocal maximum intensity projections of samples undissected mounted with water **A** or dissected mounted with water **B** or dissected and mounted with PFD **C** all with coverslips affixed. Samples continued to grow from 4 to 7 DAS only with PFD as the mounting solution. Red scale bars = 100 µm

as possible. We used the existing MorphoGraphX infrastructure to invoke custom analysis scripts [13]. We developed scripts to call different types of mesh measurement and display processes. Our main script (Additional file 6: iterative_growth_and_measures.py; https://github.com/kateharline/roeder_lab_projects/tree/master/mgx_scripts) allows users to designate which cell characteristics to measure and to specify the display and production of heatmaps with MorphoGraphX processes (Additional file 4: Video S4). The script features pauses for measures that require user input, like selecting cells for distance measures, as well as for mesh arrangement before mesh snapshotting (Additional file 4: Video S4). We also developed a script (Additional file 6: multi_resize.py; https://github.com/kateharline/roeder_lab_projects/tree/master/mgx_scripts) to address an issue with files exported from ImageJ (Additional file 5: Video S5). Sometimes the file headers are written in a way that MorphoGraphX cannot read the step size. So instead of loading an image volume, it appears as a one dimensional plane. The script iteratively opens any folder containing image files and resets the stack x, y, z dimensions to properly represent the volume, then saves the adjusted stack file. This is helpful especially if these exporting issues arise in the middle of a long term experiment when stacks need to be assembled every day to check that the entire sample was captured.

The new pipeline enables the direct quantification of cellular mechanisms of development

Combining our imaging techniques with our custom MorphoGraphX scripts enables us to capture a large dataset encompassing the early development of WT and *jaw-D* leaves (Fig. 6). From this dataset, we could analyze cell growth, division and morphology characteristics between different tissue regions, like the petiole and the margin (Fig. 7). This analysis is elaborated in our other work [22].

The *jaw-D* petioles exhibit more homogeneous growth

By labeling the cells of the petiole through the script (Additional file 6: iterative_growth_and_measures.py), we were able to compare the average growth rates and variability of growth in these cells. This uncovered that, at 7 DAS, the cells in *jaw-D* leaves exhibit greater average areal growth amongst cells and less variability between cells than WT (Fig. 7A–C). In other work, we have shown that fully grown *jaw-D* petioles are shorter than WT and that *jaw-D* mis-regulates growth anisotropy [22]. Our method is crucial in this case to differentiate between the effects of directed expansion in WT that drives petiole elongation, versus higher, yet disorganized, expansion in *jaw-D* that limits elongation.

The *jaw-D* margin is disrupted

We also used our cell labeling and quantification pipeline to explore the growth and morphology of cells at the leaf margin. The *jaw-D* leaf curling phenotype has been attributed to over-proliferation of cells at the margin [1, 23, 25, 26]. Using the script (Additional file 6: iterative_growth_and_measures.py), we selected a band of cells along the edge of leaves that we defined as the margin. Then, we quantified the growth, divisions, and characteristics of cells a prescribed distance away from this designated leaf edge. When we consider cells 10 μm or less away from the edge over time (the average width of cells from 3 to 7 DAS), we see that the average growth rates and divisions between WT and *jaw-D* leaves generally are no different (Fig. 7F–G). Only from 4 to 5 DAS and 7-8 DAS is the average areal growth different, and at 4–5 DAS it is actually higher in WT than in *jaw-D* (Student's t-test $p < 0.01$).Previously, cell cycle markers and cell density were used as a proxy for proliferation [23, 27, 28]. However, our direct measurement of cell divisions and morphology in leaf 1 suggests that, it may appear that there is more proliferation at the *jaw-D* leaf edge because margin cells are less well defined (Fig. 7D–E, H–I). In WT leaves the margin consists of elongated cells in a continuous band around the edge that may be stacked in multiple rows (Fig. 7D–E, top). While, in *jaw-D* the leaf edge exhibits some elongated cells, they can be discontinuous with gaps of small cells and usually are only one layer thick (Fig. 7D–E, bottom). When we quantify the morphology of cells 25 μm from the leaf edge (the average width of cells from 5 to 7 DAS), we find that WT cells are generally larger and longer on average (Fig. 7H–I, Student's t-test $^{*} = p < 0.05$, $^{**} = p < 0.01$).These results suggest live imaging and computational analysis is required to confirm the cellular dynamics that give rise to tissue morphology.

Conclusions

We provide an optimized method for capturing the relationship between cell and tissue morphology changes over multi-day time scales. We have conducted our experiments in the relatively fragile and morphologically dynamic early leaves of Arabidopsis WT and *jaw-D* mutant. Through our pipeline, we are able to characterize and quantify the entire leaf organ development at the cellular level. We demonstrate an analysis of two distinct leaf tissue regions, the petiole and the margin. This analysis suggests that growth homogeneity in the petiole and disrupted margin cell differentiation may contribute to the *jaw-D* leaf rippling phenotype. Our work emphasizes the importance and feasibility of measuring cell divisions, growth and

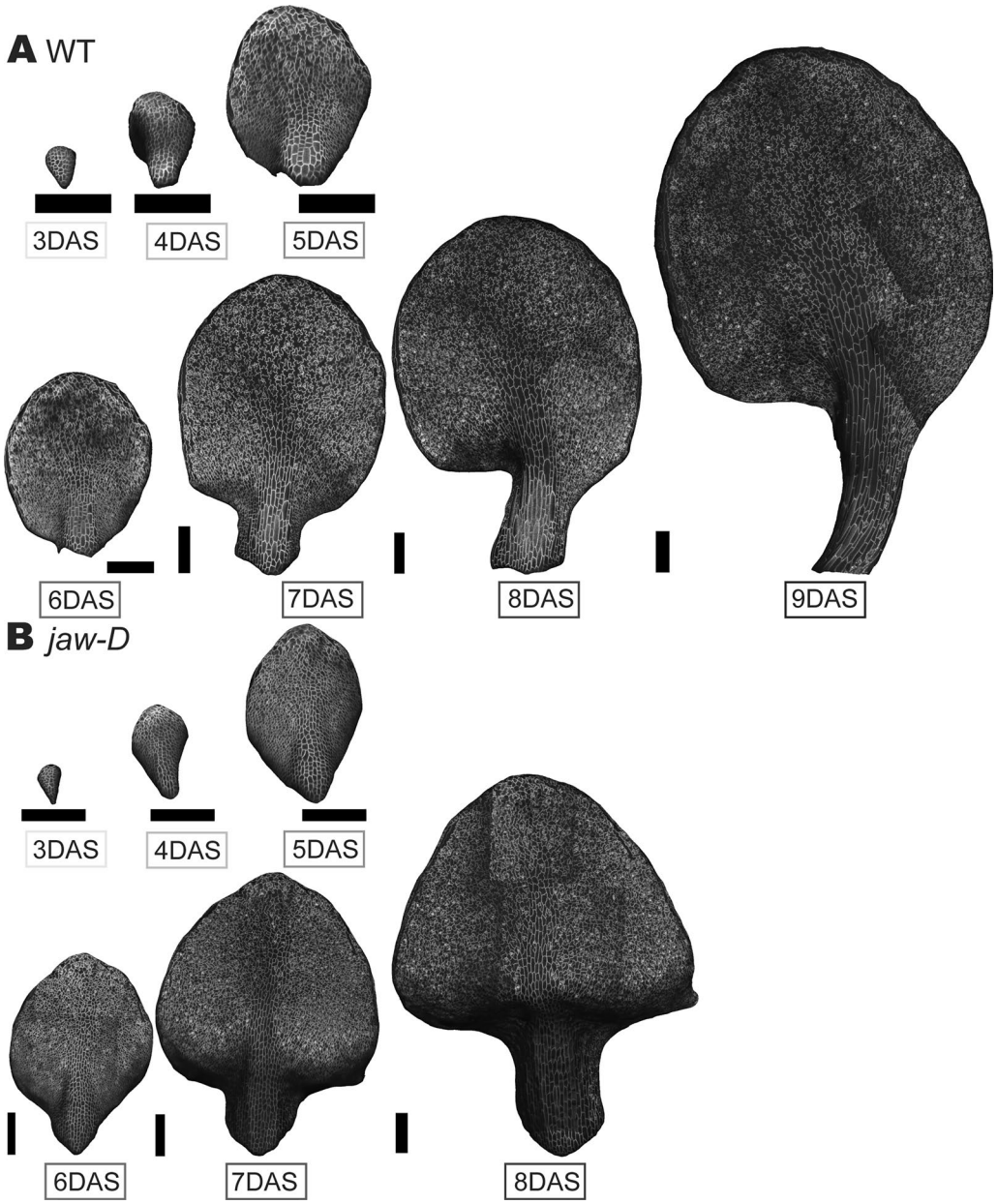

Fig. 6 Successful imaging of complex leaf development. MorphoGraphX 2.5D mesh representations of the same WT leaf imaged from 3 to 9 DAS **A** and the same *jaw-D* leaf imaged from 3 to 8 DAS **B**. The majority of the entire organ of both WT and *jaw-D* samples is visible allowing rich analysis of growth, divisions and cell types across the tissue. Black scale bar = 200 µm. This dataset was further analyzed in [22]

morphology directly in living tissues to validate and discover mechanisms of development. Our live imaging pipeline is able to capture morphologically complex tissue in a relatively straightforward, easy and quick way. We believe that our imaging technique, processing details and scripts could be applied to a variety of systems that feature morphological complexity.

Materials and methods

Plant material

WT plants are ecotype Col-0. *jaw-D* leaves are the *jaw-1D* allele originally described in [14]. Plants were crossed with the epidermal specific fluorescent reporters for plasma membrane (pAR169 *AtML1:mCitrine-RCI2a*) and nucleus (pAR229 *AtML1:H2B-TFP*) [29, 30]. These

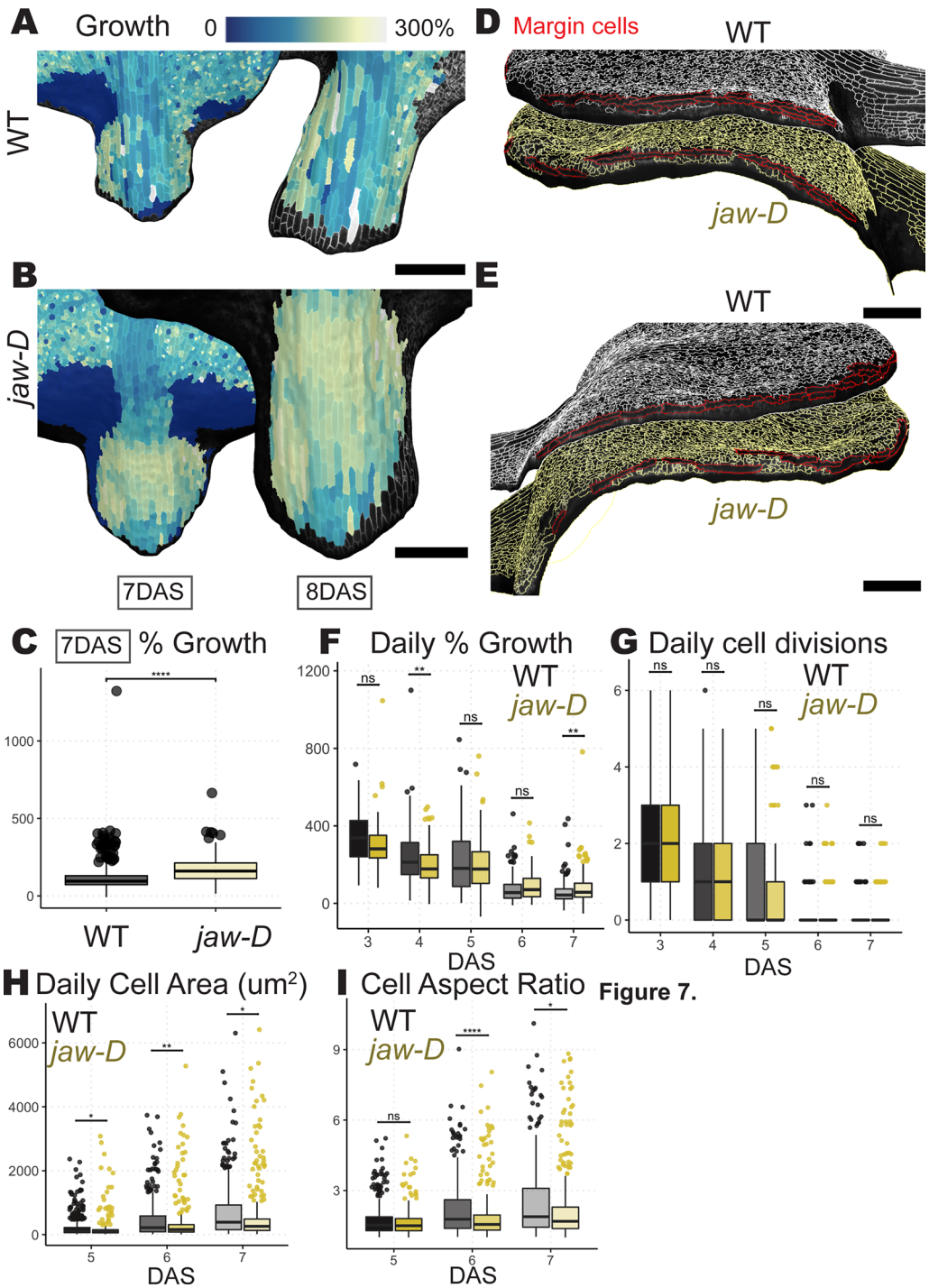

Figure 7.

Fig. 7 Pipeline can quantify petiole growth and margin patterning disruption in *jaw-D*. **A**, **B** Cell areal growth rates for 7–8 DAS displayed on 7 and 8 DAS meshes for WT **A** or *jaw-D* **B** leaf samples. **C** Quantification of areal growth rates of petiole cells. *Jaw-d* petioles have higher growth rates on average, with less variability (Student's t-test $p < 0.0001$. CV asymptotic test $p < 1.578488e{-}19$). **D**–**E** Side views of WT (top, white outlines) and *jaw-D* (bottom, yellow outlines) leaves with margin cells selected in red. Elongated margin cells form a continuous border around the edge of WT leaves, but *jaw-D* leaves have gaps. **F**–**I** Quantification of areal growth **F**, cell divisions **G**, cell area **H** and cell aspect ratio **I** for all cells 10 µm from margin from 3 to 8 DAS **F**–**G** or cells 25 µm from the margin from 5 to 7 DAS **H**–**I**. Growth and divisions are largely indistinguishable between cells at the margin between WT and *jaw-D*. Cells near the WT margin are larger and more elongated than *jaw-D*, so margin differentiation may be disrupted. (Student's t-test * = $p < 0.05$, ** = $p < 0.01$, *** = $p < 0.001$, **** = $p < 0.0001$). All measurements are from three replicates for each condition. See Tables 2, 3. for replicate cell counts

Table 2 Cells measured in WT v. *jaw-D* growth and division (Fig. 7 C, F, G)

Condition	Time point	tissue	Number of cells
WT	7 DAS	petiole	615
jaw-D	7 DAS	petiole	535
WT	3 DAS	margin	41
jaw-D	3 DAS	margin	72
WT	4 DAS	margin	122
jaw-D	4 DAS	margin	144
WT	5 DAS	margin	189
jaw-D	5 DAS	margin	117
WT	6 DAS	margin	109
jaw-D	6 DAS	margin	111
WT	7 DAS	margin	139
jaw-D	7 DAS	margin	123

Table 3 Cells measured in WT v. *jaw-D* cell characteristics (Fig. 7H, I)

Condition	Time point	Number of cells
WT	5 DAS	519
jaw-D	5 DAS	431
WT	6 DAS	337
jaw-D	6 DAS	428
WT	7 DAS	337
jaw-D	7 DAS	383

lines are available from the ABRC (pAR169 pAR229-CS73343, *jaw-D* pAR169 pAR229-CS73344). In subsequent generations, plants homozygous for both markers were selected. Note, only the plasma membrane marker was analyzed for the purposes of this paper.

Growth conditions

Plants were grown in growth chambers at 22 ℃ under continuous ~100 µmol m^{-2} s^{-1} light. Seeds were sterilized by first washing in a 70% ethanol solution supplemented with 0.01% SDS for 7–10 minutes on a nutating shaker, then at least three washes with 100% EtOH, then drying on sterile filter paper. Seeds were then plated on 60 mm petri plates with sterilized toothpicks. Growth media was 0.5× Murashige and Skoog media (pH 5.7, 0.5g/L MES, 1% phytoagar) supplemented with 1% sucrose. Plates were sealed with micropore tape. Plants were stratified at 4 ℃ for 2–7 days before being placed in the growth chamber.

Sample preparation (Fig. 1, see Table 4 for material catalog numbers)

Plants were harvested for dissection 2–3 days after being placed in the growth chamber (DAS = days after sowing) (Fig. 1A). 0-2 cotyledons were dissected off using a BD 23g 1¼ inch needle and no. 5 forceps (Fig. 1B). One cotyledon was held with the forceps, while the needle was nestled along the adaxial side of the free cotyledon until that cotyledon was sliced off. The second cotyledon was removed in a similar

Table 4 Material catalog numbers

Item	Source	Cat #
Perfluorodecalin	Sigma	P9900-25G
95% Ethanol	VWR	89,125-164
SDS	VWR	97,064-470
Whatman FILTER PAPER #1	VWR	28,450-081
Nutating mixer	Laboratory Product Sales (LPS)	S-0500
60 mm petri plates	Fisher	FB0875713A
MS media	VWR	95,025-900
MES	Fisher	47-589-3100GM
Phytoagar	Fisher	50-255-213
Sucrose	VWR	MK836006
3 M Micropore tape	Mohawk Hospital Equipment	MMM 15,301
BD 23 g 1 ¼ in needle	VWR	BD305120
Dumont Tweezer style 5 inox 8	Electron Microscopy Sciences	72,701-D
50 × 22 mm cover slips	VWR	16,004-336
Vacuum grease	VWR	59,344-055

manner, but with the stem gently steadied between the forceps. Plants were allowed to recover for 24 hours before imaging commenced. So imaging commenced either at 3 or 4 DAS. Before imaging, seedlings were arranged to expose the entire abaxial surface of one of the leaves. For our purposes, this was sufficient to study growth data on the abaxial surface. For researchers interested in comparing the first two leaves, or vegetative meristem, the sample can be placed on its side to reveal these areas. Researchers interested in the adaxial surface could explore other positions and dissections. Researchers interested in the deeper layers of the leaf would likely need more advanced microscopes or stronger fluorescent reporters (see Section "Confocal Imaging") to resolve these regions. 50×22mm coverslips were then adjusted in size (strategically broken) to fit over the arranged seedlings (Fig. 1E). Vacuum grease was extruded from a syringe without a needle onto both 22mm coverslip ends and then used to suspend the coverslip above the samples (Fig. 1D). The gap between the media and coverslip was filled with perfluorodecalin (found to be effective) or water (found not to be effective), then samples were imaged (Fig. 1C, D). Note, the coverslip remains above the samples throughout the length of the experiment to prevent fungal contamination and to keep samples well positioned, and reduce adaxial side exposure. However, in between daily imaging sessions, imaging solution was drained out from beneath the coverslip (only effective for PFD) to prevent media dissolution and sample movement. Plates were then re-sealed with micropore tape and returned to the growth chamber.

Confocal imaging

Plants were imaged on a Zeiss 710 Confocal laser scanning microscope with a 20× Plan-Apochromat NA 1.0 water immersion lens. Note, none of our air lenses could achieve a high enough resolution to resolve the fluorescent signal. The mCitrine plasma membrane marker was excited with a 514 nm argon laser and emission spectra collected from 518 to 629 (for the experiment in Figs. 3 and 5A, B) or 519–650 nm (for the experiment in Figs. 5C and 7), through a 458/514/594 (for the experiments in Figs 3, and 5A, B) or 458/514 dichroic mirror at 1–2% detector gain (for the experiment in Figs. 5C, 6 and 7). If the plants could no longer be captured within one stack, the entire visible surface of the leaf was tiled over. Cellular landmarks were used to move the sample and create small areas of overlap to ensure that every section of the leaf surface of interest is captured. Within each tile, the z-range was adjusted to minimize time imaging the leaf. When tiled manually, the cellular landmarks that overlap were used to align stacks and assemble them in MorphoGraphX 2.0 [13].

Whole plant imaging

Plants were magnified at 50× on a Zeiss Stemi 2000 stereomicroscope. Images were taken with an iPhone Max XS.

Image quality control

Over the course of live imaging experiments, each day images were inspected for quality and samples were ranked to proceed over many days based on the imaging coverage and signal level. To speed up this process, scripts in ImageJ and MorphoGraphX were implemented. In ImageJ, our tiff export script (Additional file 2: batch_tiff.py) was run on the topmost directory of the imaging files to recursively convert .lsm files from the microscope to .tiff files. Sometimes, ImageJ did not save the z-step in a format that could be read by MorphoGraphX. In this case, our stack resizing script was run in MorphoGraphX to iteratively set the z-step unit across stacks (Additional file 6: multi_resize.py, Additional file 5: Video S5). Stacks were then visually inspected in MorphoGraphX for quality. Each stack was examined in the z-direction to ensure a round glow was seen on top indicating the entire top of the sample was captured. For larger samples, each tile was aligned and assembled manually in MorphoGraphX to ensure the entire sample was captured amongst the individual images. Note, rough assemblies were used for image quality checking. Assembly was repeated more carefully for final image processing.

Image processing

Most images could be processed on an iMac Pro with Intel Xeon W 3.2 GHz 8 core CPU, 64 GB RAM, Radeon Pro Vega 64 16 GB GPU running Windows 10 through Bootcamp or a VMware Fusion Linux Virtual Machine running Ubuntu 20.04.3. The largest samples required a PC with AMD Ryzen 9 5950X 3.4 GHz 16 core CPU, 128 GB RAM, EVGA GeForce GTX Titan X 12GB Super-clocked GPU running Ubuntu 20.04.4 LTS. We found that 128 GB of RAM was necessary for processing the large samples, ~7 DAS leaves. The task list of MorphoGraphX processes and respective parameters used to create 2.5D representations of the confocal stacks are enclosed as additional files (Additional file 6: 2021_mesh_creation_mgx3.task, 2021_parent_correcting.task, Additional file 6: annotated_task_list.docx). An annotated description of tasks is also enclosed to complement MorphoGraphX documentation for new users. Briefly the image processing steps proceeded as follows. For samples exceeding a single viewing window, tiles were manually

aligned and merged in MorphoGraphX. The clipping plane tools were used to visualize and align the stacks in three dimensions. The pixel editor tool was used to erase overlapping regions to a very small sliver at the junction. Then stacks were combined using the merge process. Masks of the confocal stacks were created through 1–3 rounds of Gaussian blurring, then edge detection and closing holes in older samples where masks showed gaps. From these masks, surfaces were created, then the surface that did not contain signal was manually selected and deleted. The confocal signal was then projected onto the surface. Meshes were subdivided once, then subject to 2–3 rounds of auto-segmentation, adaptive mesh subdivision at the new cell borders and projection of the confocal signal back onto the refined mesh. Cell segmentations were manually corrected immediately after segmentation or through the process of manual cell lineage tracing and cell junction correction using the check correspondence process. Meshes from consecutive time points were manually overlaid and cell parents annotated either manually (Additional file 1: Videos S1, Additional file 2: Video S2) or using the semi-automatic parent labeling protocol. Parent tracking quality was assessed using the check correspondence function. Once meshes passed these quality control steps, we ran our iterative growth script to calculate growth and cellular parameters and produce heat map representations of the data with standardized parameters across time point comparisons and replicates (Additional file 6: iterative_growth_and_measures.py, Additional file 4: Video S4).

Data analysis

All data processing, analysis and plotting was performed in RStudio [31, 32]. Scripts used to process the data and create figures are enclosed as additional files (Additional file 6: li_preprocess.R, li_plotting.R, light_paper_plots.R) and available at https://github.com/kateharline/live_img_paper, https://github.com/kateharline/roeder_lab_projects/tree/master/imagej_scripts and https://github.com/kateharline/jawd-paper.

Supplementary Information

The online version contains supplementary material available at https://doi.org/10.1186/s13007-023-00987-2.

Additional file 1. Video S1. Parent tracking in MorphoGraphX. Two meshes from the same replicate imaging series are shown in MorphoGraphX. The cell labels are on for the first and second time point's mesh. The mesh border color is changed for the previous time point, to make cell outlines easier to see. The previous time point is scaled and laid over the subsequent time point. The parent tracking tool 'Grab label from other surface' is selected. Previous time point cells are clicked through to transfer parent labels to subsequent time point mesh. White scale bar = 200 µm (before scaling of the first mesh).

Additional file 2. Video S2. Results of parent tracking in MorphoGraphX. Two meshes from the same replicate imaging series are shown in MorphoGraphX. The cell labels are turned on for the first and second time point's mesh. The previous time point is scaled and laid over the subsequent timepoint. The corresponding parent labels are turned on for the second time point's mesh to demonstrate how the cell labels were transferred onto the successive time point. White scale bar = 200 µm (before scaling of the first mesh).

Additional file 3. Video S3. Perfluorodecalin mounting solution improves sample vitality over waterbased solutions. Animation of undissected and water submersed or dissected and water submersed or dissected and perfluorodecalin submersed samples (left to right). The growth of the first two samples begins to slow and eventually stalls from 5 to 7 DAS. The perfluorodecalin sample continues to grow. Maximum intensity projections of confocal stacks are shown false colored in green or gray. Red scale bar = 100 µm.

Additional file 4. Video S4. MorphoGraphX script (iterative_growth_and_measures.py) to rapidly quantify mesh characteristics and capture screenshots. Script parameters are edited to denote which meshes will be run, what measures will be applied, what heatmap images and mesh attributes will be saved. Both intra- and inter-mesh measures can be computed. All measures or only some can be saved as attributes for downstream analysis. The script opens each mesh in time order then conducts measures. The script exits and prompts the user to select cells from which to measure Medial-Lateral distance. Later, the script will exit to prompt the user to arrange the meshes before creating snapshots. The script creates new folders to save attribute maps of measures, snapshots and saves updated meshes.

Additional file 5. Video S5. MorphoGraphX script (multi_resize.py) to resize confocal stack voxels. Confocal stacks exported from ImageJ with z-step incorrectly recorded can appear flat in MorphoGraphX software. Users can designate which files to resize with script parameters. Users can specify voxel dimensions in script parameters. Running multi_resize.py resizes all stacks to voxel dimensions specified by the user in the script file and saves the resized stacks.

Additional file 6. Supplemental_code.zip The supplemental code file contains scripts to cary out the analysis. *batchtiff.py* is a script to convert .lsm files to .tiff files recursively through a directory. *Multi_resize.py* is a MGX script to resize voxels. *2021_mesh_creation_mgx3.task* is a MGX task list with processes for making meshes. *2021_parent_correcting.task* is a MGX task list for correcting parent labeling of meshes. *Annotated_task_list.docx* is a list of MGX processes with parameter values and notes. *Iterative_growth_and_measures.py* is a MGX script to apply various cellular measures and produce snapshots of heatmaps. *li_preprocess.R* is an R script used to preprocess data. *li_plotting.R* is an R script used to plot the data. *light_paper_plots.R* is an R script containing plot formatting.

Acknowledgements

The authors would like to thank the members of the Roeder and Smith labs for useful discussions and assistance with MorphoGraphX.

Author contributions

K.H. collected, processed and analyzed data. K.H and A.H.K.R. designed experiments, wrote and edited the manuscript. All authors read and approved the final manuscript.

Funding

Kate Harline was supported by NSF Graduate Research Fellowship (DGE-1650441). This work was funded by NSF MCB-2203275 (AHKR), The Schwartz Research Fund Award (AHKR), and the National Institute Of General Medical Sciences of the National Institutes of Health under Award Number R01GM134037 (AHKR). The content is solely the responsibility of the authors and does not necessarily represent the official views of the National Institutes of Health and other funders.

Availability of data and materials
The transgenic lines used in this work were deposited in the ABRC with stock numbers CS73343 (WT) and CS73344 (*jaw-D*). Imaging data is publicly available under a CCBY 4.0 license at the Open Science Framework. Data for Figs. 1, 2, 3, 4, 5A, B is available at https://doi.org/10.17605/OSF.IO/V2TKW. Data for Figs. 5C, 6 and 7 is available at https://doi.org/10.17605/OSF.IO/D7X3Y.

Declarations

Ethics approval and consent to participate
Not applicable

Consent for publication
Not applicable

Competing interests
The authors declare that they have no competing interests.

Received: 27 November 2022 Accepted: 21 January 2023
Published online: 01 February 2023

References

1. Avery GS. Structure and development of the tobacco leaf. Am J Bot. 1933;20:565.
2. Poethig RS, Sussex IM. The developmental morphology and growth dynamics of the tobacco leaf. Planta. 1985;165:158–69.
3. Derr J, Bastien R, Couturier É, Douady S. Fluttering of growing leaves as a way to reach flatness: experimental evidence on Persea americana. J R Soc Interface. 2018. https://doi.org/10.1098/rsif.2017.0595.
4. Armon S, Moshe M, Sharon E. The multiscale nature of leaf growth fields. Commun Phys. 2021;4:122.
5. Remmler L, Rolland-Lagan A-G. Computational method for quantifying growth patterns at the adaxial leaf surface in three dimensions. Plant Physiol. 2012;159:27–39.
6. Elsner J, Michalski M, Kwiatkowska D. Spatiotemporal variation of leaf epidermal cell growth: a quantitative analysis of Arabidopsis thaliana wild-type and triple cyclinD3 mutant plants. Ann Bot. 2012;109:897–910.
7. Kierzkowski D, Runions A, Vuolo F, Strauss S, Lymbouridou R, Routier-Kierzkowska A-L, et al. A growth-based framework for leaf shape development and diversity. Cell. 2019;177:1405-1418.e17.
8. Fox S, Southam P, Pantin F, Kennaway R, Robinson S, Castorina G, et al. Spatiotemporal coordination of cell division and growth during organ morphogenesis. PLoS Biol. 2018;16:e2005952.
9. Calder G, Hindle C, Chan J, Shaw P. An optical imaging chamber for viewing living plant cells and tissues at high resolution for extended periods. Plant Methods. 2015;11:22.
10. Caggiano MP, Yu X, Ohno C, Sappl P, Heisler MG. Live imaging of arabidopsis leaf and vegetative meristem development. Methods Mol Biol. 2021;2200:295–302.
11. Roeder AHK, Tarr PT, Tobin C, Zhang X, Chickarmane V, Cunha A, et al. Computational morphodynamics of plants: integrating development over space and time. Nat Rev Mol Cell Biol. 2011;12:265–73.
12. Harline K, Martínez-Gómez J, Specht CD, Roeder AHK. A life cycle for modeling biology at different scales. Front Plant Sci. 2021;12:710590.
13. Strauss S, Runions A, Lane B, Eschweiler D, Bajpai N, Trozzi N, et al. Using positional information to provide context for biological image analysis with MorphoGraphX 2.0. Elife. 2022. https://doi.org/10.7554/eLife.72601.
14. Palatnik JF, Allen E, Wu X, Schommer C, Schwab R, Carrington JC, et al. Control of leaf morphogenesis by microRNAs. Nature. 2003;425:257–63.
15. White DWR. PEAPOD regulates lamina size and curvature in Arabidopsis. Proc Natl Acad Sci USA. 2006;103:13238–43.
16. Serrano-Cartagena J, Candela H, Robles P, Ponce MR, Pérez-Pérez JM, Piqueras P, et al. Genetic analysis of incurvata mutants reveals three independent genetic operations at work in Arabidopsis leaf morphogenesis. Genetics. 2000;156:1363–77.
17. Goodrich J, Puangsomlee P, Martin M, Long D, Meyerowitz EM, Coupland G. A Polycomb-group gene regulates homeotic gene expression in Arabidopsis. Nature. 1997;386:44–51.
18. Pawley J. Handbook Of Biological Confocal Microscopy. 3rd ed. New York: Springer; 2006.
19. Grandjean O, Vernoux T, Laufs P, Belcram K, Mizukami Y, Traas J. In vivo analysis of cell division, cell growth, and differentiation at the shoot apical meristem in Arabidopsis. Plant Cell. 2004;16:74–87.
20. Reddy GV, Roy-Chowdhury A. Live-imaging and image processing of shoot apical meristems of Arabidopsis thaliana. Methods Mol Biol. 2009;553:305–16.
21. Hamant O, Das P, Burian A. Time-lapse imaging of developing shoot meristems using a confocal laser scanning microscope. Methods Mol Biol. 2019;1992:257–68.
22. Harline K, Fruleux A, Lane B, Mosca G, Strauss S, Tavakolian N, et al. Dynamic growth re-orientation orchestrates flatness in the Arabidopsis leaf. BioRxiv. 2022;4(2):122.
23. Alvarez JP, Furumizu C, Efroni I, Eshed Y, Bowman JL. Active suppression of a leaf meristem orchestrates determinate leaf growth. Elife. 2016. https://doi.org/10.7554/eLife.15023.
24. Littlejohn GR, Gouveia JD, Edner C, Smirnoff N, Love J. Perfluorodecalin enhances in vivo confocal microscopy resolution of Arabidopsis thaliana mesophyll. New Phytol. 2010;186:1018–25.
25. Challa KR, Rath M, Nath U. The CIN-TCP transcription factors promote commitment to differentiation in Arabidopsis leaf pavement cells via both auxin-dependent and independent pathways. PLoS Genet. 2019;15:e1007988.
26. Rebocho AB, Southam P, Kennaway JR, Bangham JA, Coen E. Generation of shape complexity through tissue conflict resolution. Elife. 2017. https://doi.org/10.7554/eLife.20156.
27. Efroni I, Blum E, Goldshmidt A, Eshed Y. A protracted and dynamic maturation schedule underlies Arabidopsis leaf development. Plant Cell. 2008;20:2293–306.
28. Beltramino M, Ercoli MF, Debernardi JM, Goldy C, Rojas AML, Nota F, et al. Robust increase of leaf size by Arabidopsis thaliana GRF3-like transcription factors under different growth conditions. Sci Rep. 2018;8:13447.
29. Robinson DO, Coate JE, Singh A, Hong L, Bush M, Doyle JJ, et al. Ploidy and size at multiple scales in the Arabidopsis sepal. Plant Cell. 2018;30:2308–29.
30. Roeder AHK, Chickarmane V, Cunha A, Obara B, Manjunath BS, Meyerowitz EM. Variability in the control of cell division underlies sepal epidermal patterning in Arabidopsis thaliana. PLoS Biol. 2010;8:e1000367.
31. RStudio Team. RStudio. 2020 RStudio: Integrated Development for R. http://www.rstudio.com/. Accessed 13 Apr 2022.
32. R Core Team. 2021 R: The R Project for Statistical Computing. https://www.R-project.org/. Accessed 13 Apr 2022.

Publisher's Note